

Diffusive Magnon Spin Nernst Effect in Antiferromagnets

Hantao Zhang¹ and Ran Cheng^{1,2}

¹*Department of Electrical and Computer Engineering,
University of California, Riverside, CA 92521, USA*

²*Department of Physics and Astronomy, University of California, Riverside, CA 92521, USA*

Magnon spin Nernst effect was recently proposed as an intrinsic effect in antiferromagnets, where spin diffusion and boundary spin transmission have been ignored. However, diffusion processes are essential to convert a bulk spin current into boundary spin accumulation, which determines the spin injection rate into detectors through imperfect transmission. We formulate a diffusive theory of the magnon spin Nernst effect with boundary conditions reflecting real device geometry. Thanks to the diffusion effect, the output signals in both electronic and optical detection grow rapidly with an increasing system size in the transverse dimension, which eventually saturate. Counterintuitively, the measurable signals are even functions of magnetic field, yielding optical detection more reliable than electronic detection.

With the rapid growth of nano-electronics, it becomes increasingly demanding to develop energy-efficient means to process and transmit information. Magnons—the quanta of spin wave excitations—are promising alternative to electrons because they are charge neutral and can transport spin angular momenta in insulating materials without incurring Joule heating [1]. While ferromagnetic (FM) magnons exhibit fixed spin polarization determined solely by the magnetization, antiferromagnetic (AFM) magnons can carry both spin-up and spin-down polarizations similar to electrons [2–5], forming an internal degree of freedom capable of encoding digital 0 and 1. This unique property, along with the ultrafast spin dynamics, insensitivity to magnetic disturbance, have fertilized AFM magnonics as a prosperous frontier in materials sciences [6].

In two dimensions, a prominent phenomenon demonstrating spin-contrasting physics is the spin Hall effect (SHE). Concerning spin transport, the similarity between AFM magnons and electrons enables the magnonic analog of the SHE, known as the magnon spin Nernst effect (SNE) [7–9]. To detect the SHE, it is essential to consider the spin diffusion process that converts a spin current into boundary spin accumulations [10]. However, the magnon SNE has been proposed as an intrinsic effect where spin diffusion has been completely ignored. A non-diffusive picture also fails to capture the imperfect transmission of spin angular momenta between AFM magnons and metallic contacts, which is essential to the electronic detection of magnon SNE. Moreover, unlike the magnon thermal Hall effect [11–13], the magnon SNE is not accompanied by chiral edge currents [7, 8], thus boundary spin accumulations solely arise from bulk spin currents through the diffusion process. Therefore, a correct understanding of the magnon SNE calls for a diffusive description of magnons in AFM materials.

In this Letter, we formulate a diffusive theory of the magnon SNE in a finite two-dimensional AFM insulator with realistic boundary conditions. We first consider a prototype device geometry illustrated in Fig. 1, where the

transverse boundaries are directly contacted to metallic leads. Driven by an applied temperature gradient, magnons with opposite spins diffuse towards opposite transverse boundaries and inject pure spin currents into the leads. The injected spins are subsequently converted into a charge voltage by the inverse SHE, producing an actual measurable signal. We find that the voltage output grows appreciably with an increasing system width until it eventually saturates. We then consider an isolated AFM insulator amenable to optical detection as illustrated in Fig. 3, where magnons accumulate on dead ends but do not inject into leads. For both types of device geometry, we find that the detectable signals are even functions of the applied magnetic field along the Néel order (orthogonal to the plane). This is in sharp contrast to what one would naively obtain from a non-diffusive description. Consequently, it becomes fundamentally difficult to separate the inverse SHE voltage from the ubiquitous thermoelectric signal, thus optical detection is favored over electronic detection.

Magnon spin diffusion.—Without loss of generality, let us consider a two dimensional AFM with collinear Néel order perpendicular to the plane. The existence of magnon SNE calls for special symmetry breaking and the ensuing Dzyaloshinskii-Moriya interaction, but the microscopic mechanism does not concern us here in a diffusive description. As illustrated in Fig. 1, a temperature gradient ∇T applied along the x direction generates a pure spin current $j_s = -\sigma_s \nabla T$ in the y direction, where the SNE coefficient σ_s is a bulk quantity independent of boundaries. To solve the magnon spin diffusion in the y direction, we make the following assumptions: 1) magnons of different spin species relax to the environment (phonons) individually without spin-flip scattering between magnons; 2) the momentum relaxation ascribing to spin-preserving processes is orders of magnitude faster than the spin relaxation due to spin-non-preserving processes. As a result, we are able to decouple the spin diffusion equations for each spin species, equating the magnon temperature to the environmental temperature

locally, and only keep the $\partial_x T$ component which is fixed externally. In the natural units ($\hbar = k_B = e = 1$), the current density of spin-up magnons is

$$j_y^\uparrow = -\sigma_\uparrow \partial_x T - D_\uparrow \partial_y \rho_\uparrow \quad (1)$$

where ρ_\uparrow is the density of spin-up magnons, D_\uparrow is the magnon diffusivity, and σ_\uparrow is the Nernst coefficient for spin-up magnons. The equation for j_y^\downarrow is similar and the total spin current density $j_s = j_\uparrow - j_\downarrow$ and $\sigma_s = \sigma_\uparrow - \sigma_\downarrow$. In the absence of magnetic fields, $\sigma_\uparrow = -\sigma_\downarrow$, $D_\uparrow = D_\downarrow$, and $\rho_\uparrow = \rho_\downarrow$ guaranteed by symmetry. A magnetic field perpendicular to the plane can break this symmetry, which will be discussed in the following.

Since we have ignored the spin-flip scattering between magnons with opposite spins, the spin continuity equation is respected separately by each spin species

$$\frac{\partial \rho_\gamma}{\partial t} + \nabla \cdot \mathbf{j}^\gamma = -\frac{\rho_\gamma}{\tau_\gamma}, \quad (2)$$

where $\gamma = \uparrow, \downarrow$ and τ_γ is the effective spin-relaxation time due to spin-non-conserving scattering with phonons, impurities, etc. We treat τ_γ as a phenomenological parameter; $\tau_\uparrow = \tau_\downarrow$ in the absence of magnetic fields. We will focus on the linear response regime such that the spatial inhomogeneity of transport coefficients in Eq. (1) is negligible, which requires $|L \partial_x T / T| \ll 1$ with L the length in the x direction (see Fig. 1). At steady state, $\partial \rho_\gamma / \partial t = 0$, then inserting Eq. (1) into Eq. (2) gives $\nabla^2 \rho_\gamma = \rho_\gamma / \lambda_\gamma^2$, where $\lambda_\gamma = \sqrt{D_\gamma \tau_\gamma}$ is the effective spin diffusion length for spin γ . When the system width w far exceeds its length L , the diffusion process becomes effectively a one dimensional problem. Therefore,

$$\frac{\partial^2 \rho_\gamma}{\partial y^2} = \frac{\rho_\gamma}{\lambda_\gamma^2}, \quad (3)$$

which requires two boundary conditions to solve for each γ . In the right (left) leads, the spin density of electrons ρ_R (ρ_L) satisfies the same diffusion equation governed by a different spin diffusion length $\lambda_e = \sqrt{D_e \tau_e}$ where D_e is the spin diffusivity and τ_e is the spin relaxation time of electrons.

Solving Eq. (3) together with the spin diffusion equations for $\rho_{R/L}$ calls for proper boundary conditions determined by the interfacial spin transmission between magnons and electrons. As illustrated in Fig. 1, there exists four different scattering processes, each involving an electron that releases an angular momentum of either \hbar or $-\hbar$ through spin-flip and a magnon that balances the change of the electron spin. Specifically, in the absence of magnetic fields, the process (a) emitting spin-up magnons and the process (b) absorbing spin-down magnons form a time-reversal pair, which take place with the same rate, so do (c) and (d). These four interfacial processes are characterized by four conductance parameters that can be calculated by the linear response theory [5, 14]. Assuming identical interfacial properties and

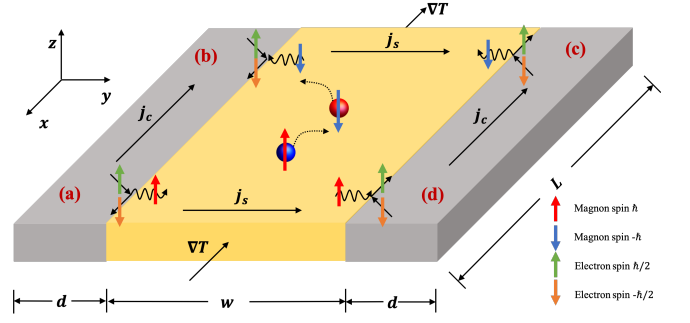


FIG. 1. Illustration of system geometry and spin transmission processes at boundaries. A temperature gradient ∇T along x generates a transverse pure spin current \mathbf{j}_s through the SNE in the AFM (yellow region). The spin current injects into the metallic leads (grey region) on both sides through four different spin transmission processes labeled as (a)–(d). The injected spin currents are converted into detectable voltages along x through the inverse SHE in the leads. The system length along x is L ; the AFM width and the lead width are w and d , respectively.

detailed balance, we can reduce the four parameters into two such that (a) and (d) [(b) and (c)] are represented by the same conductance G_\uparrow (G_\downarrow) [15]. For example, on the right interface ($y = w/2$), the Ohm's law associated with (c) and (d) determines two spin current densities crossing the interface: $j_{\text{int}}^\uparrow = G_\uparrow [\rho_\uparrow(w/2) - \rho_R(w/2)]$ and $j_{\text{int}}^\downarrow = G_\downarrow [\rho_\downarrow(w/2) - (-\rho_R(w/2))]$. Spin continuity requires that $j_{\text{int}}^\uparrow = j_y^\uparrow(w/2)$ and $j_{\text{int}}^\downarrow = j_y^\downarrow(w/2)$, and that $j_{\text{int}}^\uparrow - j_{\text{int}}^\downarrow = -D_e \left. \frac{\partial \rho_R}{\partial y} \right|_{w/2}$. These relations constitute three independent conditions at $x = w/2$. Similarly, there are three boundary conditions arising from the processes (a) and (b) on the opposite interface at $x = -w/2$. At the dead ends $y = \pm(w/2 + d)$ with d the lead width, spin currents must vanish identically, which provides another two independent conditions. Including everything, we finally obtain a set of eight boundary conditions grouped into four relations as

$$G_\gamma \left[\rho_L \mp \rho_\gamma \left(-\frac{w}{2} \right) \right] = \pm j_y^\gamma \left(-\frac{w}{2} \right), \quad (4a)$$

$$G_\gamma \left[\rho_R \mp \rho_\gamma \left(-\frac{w}{2} \right) \right] = \mp j_y^\gamma \left(-\frac{w}{2} \right), \quad (4b)$$

$$-D_e \left. \frac{\partial \rho_{R/L}}{\partial y} \right|_{\pm w/2} = j_y^\uparrow \left(\pm \frac{w}{2} \right) - j_y^\downarrow \left(\pm \frac{w}{2} \right), \quad (4c)$$

$$-D_e \left. \frac{\partial \rho_{R/L}}{\partial y} \right|_{\pm(w/2+d)} = 0, \quad (4d)$$

where $\gamma = \uparrow$ (\downarrow) in Eq. 4a and 4b and R (L) in Eq. (4c) and (4d) are linked to the upper (lower) sign of \pm and \mp appearing in these equations. It should be noted that G_γ is the same on both boundaries and independent of ρ_γ and $\rho_{R/L}$, which is true in the linear response regime for identical leads on both sides. Invoking the above boundary conditions on the spin diffusion Eq. (3), we

are able to solve the magnon density $\rho_\uparrow(y)$ and $\rho_\downarrow(y)$ for $-w/2 < y < w/2$ as well as the electron spin density $\rho_L(y)$ and $\rho_R(y)$ for $-(w/2 + d) < y < -w/2$ and $w/2 < y < w/2 + d$, respectively.

Electronic Detection.—In the leads, the inverse SHE converts the injected spin angular momenta into an electrical current $\mathbf{j}_{L/R} = \sigma_c[\mathbf{E}_{L/R} - \theta_s/(eg_F)\hat{z} \times \nabla \rho_{L/R}]$ [16], where σ_c is the conductivity of the leads, $\mathbf{E}_{L/R}$ is the electric field, and θ_s is the spin Hall angle, and g_F is the density of states at the Fermi level. With the open boundary condition $\mathbf{j}_{L/R} = 0$, the inverse SHE generates a voltage $V_{L/R} = L/d \int dy E_{L/R}$ along the x direction. If the two leads are made of identical materials and the interfacial properties are the same on both sides, symmetry guarantees that $V_L = V_R = V$ under the SHE geometry. In the absence of magnetic fields, time-reversal symmetry guarantees that $\sigma = \sigma_\uparrow = -\sigma_\downarrow$, $\lambda_m = \lambda_\uparrow = \lambda_\downarrow$, $D_m = D_\uparrow = D_\downarrow$, and $G = G_\uparrow = G_\downarrow$. Retrieving all physical constants from the natural units, we obtain

$$V = -\partial_x T \frac{\sigma \theta_s L}{eGd} \frac{\eta_m \eta_e \tanh \frac{d}{2\lambda_e}}{\eta_m + \coth \frac{w}{2\lambda_m} \left(1 + 2\eta_e \coth \frac{d}{\lambda_e}\right)}, \quad (5)$$

where e is the electron charge, $\eta_m = G\lambda_m/D_m$ and $\eta_e = G\lambda_e/D_e$ are dimensionless parameters, and w , d , and L describe the device geometry illustrated in Fig. 1. The spin diffusion effect of magnons is reflected in the ratio w/λ_m , while d/λ_e affecting the electron spin diffusion in the leads can be varied independently. In the ballistic limit that $w \ll \lambda_m$, the $\coth w/2\lambda_m$ factor in the denominator of Eq. (5) blows up, thus the actual output voltage is highly suppressed. To linear order in w/λ_m , we have $V = -\partial_x T (wL/2d)(\sigma\theta_s/eD_m)\eta_e \tanh(d/2\lambda_e)/[1 + 2\eta_e \coth(d/\lambda_e)]$, which is linear in w . On the other hand, when both magnons and electrons are in the diffusive limit, *i.e.* $w \gg \lambda_m$ and $d \gg \lambda_e$, Eq. 5 becomes

$$V = -\partial_x T \frac{\sigma \theta_s L}{ed} \frac{G\lambda_e \lambda_m}{D_e D_m + G(D_e \lambda_m + 2D_m \lambda_e)}, \quad (6)$$

which is independent of w . Figure 2 plots the output V as a function of w/λ_m and d/λ_e for typical materials parameters of MnPS₃ (see the SI). The essential pattern of Fig. 2 is preserved even by varying η_m and η_e . While V increases monotonically towards saturation with an increasing w/λ_m , it varies non-monotonically with d/λ_e , where the maximum appears for d being comparable to λ_e . These features suggest that: 1) The diffusion effect of magnons can significantly facilitate the electronic detection of the magnon SNE. The saturation voltage output for $w \gg \lambda_m$ can be orders of magnitude larger than that in the ballistic limit. 2) The spin diffusion of electrons in the leads can either enhance or suppress the output, so the dimensions and the material properties of the leads should be optimized.

The fact that the output voltage in both leads are the same makes it difficult to separate the magnon SNE from

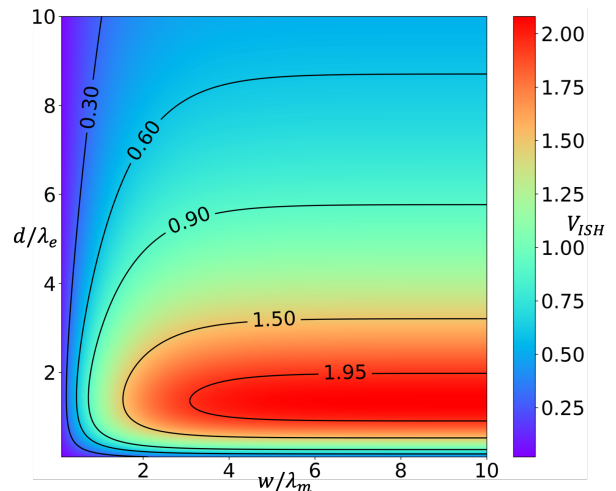


FIG. 2. Inverse SHE voltage resulting from the spin currents injected into the leads as a function of w/λ_m and d/λ_e for $\eta_m = \eta_e = 16$, which is estimated by using materials parameters in MnPS₃ (see the SI). Unit: $-\partial_x T(\sigma\theta_s L/eG\lambda_e)$.

thermoelectric effects. Therefore, it is natural to consider applying a magnetic field perpendicular to the plane to break the degeneracy of the spin-up and spin-down magnons. However, a scrutiny over the spin transmission processes in Fig. 1 suggests a negative conclusion. Suppose that the Zeeman interaction lowers the gap of spin-up magnon band, enlarging its population, whereas spin-down magnons experience the opposite change. In the linear response regime, the intensity of process (a) dubbed I_a and that of process (d) dubbed I_d will increase by exactly the same amount ΔI_+ . Similarly, I_b and I_c will decrease by the same amount ΔI_- . Accordingly, the total amount of spin injection from the left lead, determined by $I_a + I_b$, will change by $\Delta I_+ - \Delta I_-$. This is exactly the same as the change of spin injection into the right lead determined by $I_c + I_d$. In other words, an applied magnetic field causes the same change in both leads, hence the output voltage V must be quadratic in the magnetic field.

Now we justify the above conclusion by expanding the inverse SHE voltages V_L and V_R arising from the two leads with respect to B . For weak fields, $\sigma_\gamma = \sigma \pm \sigma' B + \sigma'' B^2/2$ where $\sigma' = \partial_B \sigma(0)$, $\sigma'' = \partial_B^2 \sigma(0)$, and the $+$ ($-$) sign corresponds to $\gamma = \uparrow$ (\downarrow). Similar expansions apply to all other parameters such as η_m and η_e . Solving V_L and V_R from Eq. (3) under spin-specific boundary conditions (*i.e.*, $\gamma = \uparrow$ or \downarrow in Eq. (4)), we find that the linear term of B vanishes identically in both V_L and V_R while they share the same B^2 term. Therefore, we have $V_L = V_R = V(B)$ even in the presence of a magnetic field. Letting $\Delta V \equiv V(B) - V(0)$, we obtain

$$\frac{\Delta V}{V(0)} = \frac{B^2}{\eta_m \sigma \mathfrak{D}} \left(\frac{a}{1 + \eta_m} + b + c \right), \quad (7)$$

where $\mathcal{D} = 1 + \eta_m + 2\eta_e$, $a = -\eta_m^2\sigma(1 + 2\eta_e) + 2\eta_m'(\eta_m\eta_e'\sigma + \eta_e\sigma')$, $b = \eta_m''\sigma/2 + \eta_m(1 + \eta_m)\sigma''/2 + \eta_m'\sigma'$, and $c = \eta_m''\eta_e\sigma - \eta_m\eta_e''\sigma + \eta_m\eta_e\sigma''$. In the expansions, we have ignored the very insensitive field dependence of θ_s , D_e and λ_e . Since a magnetic field cannot make V_L and V_R different, electronic detection of the magnon SNE turns out to be an unreliable approach.

Optical Detection.—The boundary spin accumulation arising from the magnon SNE can be detected optically without metallic leads. Accordingly, we use $j_\gamma(\pm w/2) = 0$ as the boundary conditions and solve the magnon spin density $\rho_s = \rho_\uparrow - \rho_\downarrow$ from Eq. (3) as

$$\rho_s(y) = -2\partial_x T \frac{\sigma\lambda_m}{D_m} \operatorname{sech}\frac{w}{2\lambda_m} \sinh\frac{y}{\lambda_m}, \quad (8)$$

which is plotted in Fig. 3. Because $\rho_s(y) = -\rho_s(-y)$ is an odd function, the profile can be unambiguously probed via spin-resolved magnon-photon interactions if the spatial resolution is higher than $1/w$. Typical optical measurements are not able to discern $\rho_\uparrow(y)$ and $\rho_\downarrow(y)$ individually; only the spin density $\rho_s(y)$ can be measured. On the edges, $\rho_s(\pm w/2) \sim \pm \tanh(w/2\lambda_m)$, which increases with an increasing ratio of w/λ_m until it eventually saturates. This behavior, shown in the inset of Fig. 3, is similar to the case of electronic detection.

Although thermoelectric effects are no longer a concern in optical detection, it is instructive to examine how ρ_s depends on a perpendicular magnetic field B . In the diffusive limit that $w \gg \lambda_\gamma$ ($\gamma = \uparrow, \downarrow$), we expand the spin-dependent quantities up to quadratic order in B . The change of ρ_s on the right edge $\Delta\rho_s = \rho_s(B, w/2) - \rho_s(0, w/2)$ is obtained as

$$\frac{\Delta\rho_s}{\rho_s^0} = B^2 \frac{(\zeta\sigma)''}{2\zeta\sigma} \quad (9)$$

where $\rho_s^0 = \rho_s(0, w/2)$, $\zeta = \lambda_m/D_m$, and σ are defined for $B = 0$; $\zeta'' = \partial_B^2\zeta(0)$ and $\sigma'' = \partial_B^2\sigma(0)$. Similar to the electronic detection, the change of magnon spin density on each boundary is an even function of B , so it does not matter if a magnetic field is applied along the z or the $-z$ direction. However, we are not able to determine the sign of $(\zeta\sigma)''/\zeta\sigma$ in Eq. (9), so a perpendicular magnetic field can either enhance or suppress the boundary spin accumulation depending on materials.

To better visualize the influence of magnetic field, we exaggerate the changes of ζ and σ induced by B in plotting the profile of $\rho_s(y)$ in Fig. 3. In fact, the quadratic B -dependence and the anti-symmetric spatial distribution of the spin density, is not unique to the magnon SNE in AFM. It was also observed in the electron SHE under optical detection [17].

Materials Estimate.—Comparing with the electronic detection where the output voltage is difficult to be separated from thermoelectric effects even in the presence of magnetic field, optical detection turns out to be the

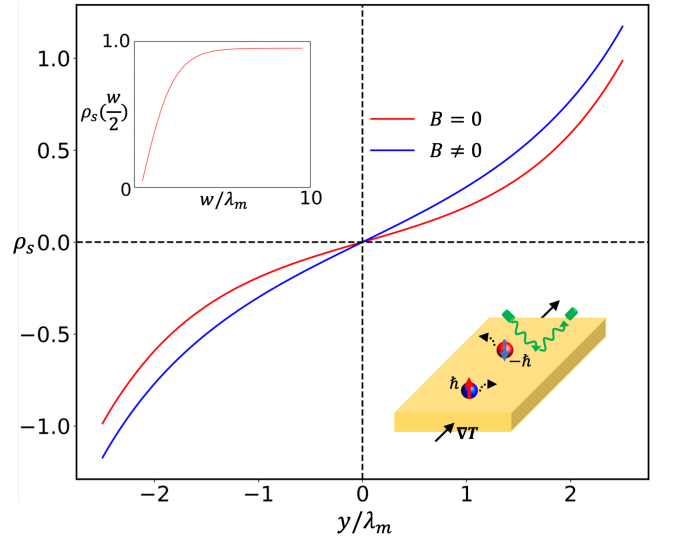


FIG. 3. Magnon spin density ρ_s as a function of y for open boundaries and $w = 5\lambda_m$. Insets: Magnon spin density on the edge $\rho_s(w/2)$ as a function of w/λ_m (upper-left); illustration of device geometry (lower-right). Unit: $-2\partial_x T(\sigma\lambda_m/D_m)$.

preferred method to observe the diffusive magnon SNE thanks to the anti-symmetric profile of $\rho_s(y)$.

Magneto-optic Kerr effect microscopy is a well-established optical detection [17–19], but it does not provide enough spatial resolution to measure systems on or below the micrometer scale. Recent development in the nitrogen-vacancy (NV) center magnetometer [20–24], on the other hand, exhibits remarkable sensitivity combined with a high spatial resolution, making it quite promising to measure the spatial profile of $\rho_s(y)$, hence the magnon SNE.

While the magnon SNE was theoretically predicted and experimentally explored in MnPS_3 [7, 9], recent studies suggest that its variance (such as CrSiTe_3) can exhibit a much larger SNE coefficient [25]. Therefore, we choose the largest reported value, $\sigma_\uparrow = \sigma_\downarrow \approx 2.5 \times 10^{-2} k_B/\hbar$, for estimation. In the absence of magnetic fields, we take $\tau_m \approx 10\text{ns}$ [26], $\lambda_m \approx 1\mu\text{m}$ [27], and $w \gg \lambda_m$. For a thin film consisting of about 10 layers [28], a temperature gradient $\partial_x T$ on the order of $10^5 \sim 10^6 \text{K/m}$ will produce an areal spin density of roughly $10^{13} \sim 10^{14} \hbar/\text{m}^2$ on the edge. Assuming a pixel size of $20\text{nm} \times 20\text{nm}$ and a distance of 20nm between the NV center and the material surface [21], we estimate that the edge spin accumulation of magnons will generate a static magnetic field acting on the NV center on the order of $1 \sim 10\text{nT}$, which is within the sensitivity [24].

In summary, we have formulated a diffusive theory of the magnon SNE in antiferromagnets with collinear Néel order, providing experimentally measurable predictions missed in previous theoretical studies. Owing to the magnetoelectric effects which mixes with the output voltage,

optical detection turns out to be more reliable than electronic detection. The NV center magnetometer is able to fulfill this function.

We acknowledge inspiring discussions with X. Chen, C. Du, and A. Balandin. This work is supported by the Air Force Office of Scientific Research under grant FA9550-19-1-0307.

-
- [1] S. Maekawa, S. O. Valenzuela, E. Saitoh, and T. Kimura, *Spin Current* (Oxford University Press, 2017).
- [2] F. Keffer and C. Kittel, Theory of antiferromagnetic resonance, *Physical Review* **85**, 329 (1952).
- [3] F. Keffer, H. Kaplan, and Y. Yafet, Spin waves in ferromagnetic and antiferromagnetic materials, *American Journal of Physics* **21**, 250 (1953).
- [4] S. Rezende, R. Rodríguez-Suárez, and A. Azevedo, Diffusive magnonic spin transport in antiferromagnetic insulators, *Physical Review B* **93**, 054412 (2016).
- [5] K. Chen, W. Lin, C. Chien, and S. Zhang, Temperature dependence of angular momentum transport across interfaces, *Physical Review B* **94**, 054413 (2016).
- [6] V. Baltz, A. Manchon, M. Tsoi, T. Moriyama, T. Ono, and Y. Tserkovnyak, Antiferromagnetic spintronics, *Reviews of Modern Physics* **90**, 015005 (2018).
- [7] R. Cheng, S. Okamoto, and D. Xiao, Spin nernst effect of magnons in collinear antiferromagnets, *Physical review letters* **117**, 217202 (2016).
- [8] V. A. Zyuzin and A. A. Kovalev, Magnon spin nernst effect in antiferromagnets, *Physical review letters* **117**, 217203 (2016).
- [9] Y. Shiomi, R. Takashima, and E. Saitoh, Experimental evidence consistent with a magnon nernst effect in the antiferromagnetic insulator mnps_3 , *Physical Review B* **96**, 134425 (2017).
- [10] S. Zhang, Spin hall effect in the presence of spin diffusion, *Physical review letters* **85**, 393 (2000).
- [11] R. Matsumoto, R. Shindou, and S. Murakami, Thermal hall effect of magnons in magnets with dipolar interaction, *Physical Review B* **89**, 054420 (2014).
- [12] S. K. Kim, H. Ochoa, R. Zarzuela, and Y. Tserkovnyak, Realization of the haldane-kane-mele model in a system of localized spins, *Physical review letters* **117**, 227201 (2016).
- [13] A. Rückriegel, A. Brataas, and R. A. Duine, Bulk and edge spin transport in topological magnon insulators, *Physical Review B* **97**, 081106 (2018).
- [14] S. S.-L. Zhang and S. Zhang, Spin convertance at magnetic interfaces, *Physical Review B* **86**, 214424 (2012).
- [15] R. E. Troncoso, S. A. Bender, A. Brataas, and R. A. Duine, Spin transport in thick insulating antiferromagnetic films, *Physical Review B* **101**, 054404 (2020).
- [16] R. Cheng, J.-G. Zhu, and D. Xiao, Dynamic feedback in ferromagnet–spin hall metal heterostructures, *Physical review letters* **117**, 097202 (2016).
- [17] Y. K. Kato, R. C. Myers, A. C. Gossard, and D. D. Awschalom, Observation of the spin hall effect in semiconductors, *science* **306**, 1910 (2004).
- [18] O. van ‘t Erve, A. Hanbicki, K. McCreary, C. Li, and B. Jonker, Optical detection of spin hall effect in metals, *Applied Physics Letters* **104**, 172402 (2014).
- [19] C. Stamm, C. Murer, M. Berritta, J. Feng, M. Gabureac, P. M. Oppeneer, and P. Gambardella, Magneto-optical detection of the spin hall effect in pt and w thin films, *Physical review letters* **119**, 087203 (2017).
- [20] J. Taylor, P. Cappellaro, L. Childress, L. Jiang, D. Budker, P. Hemmer, A. Yacoby, R. Walsworth, and M. Lukin, High-sensitivity diamond magnetometer with nanoscale resolution, *nature physics* **4**, 810 (2008).
- [21] P. Maletinsky, S. Hong, M. S. Grinolds, B. Hausmann, M. D. Lukin, R. L. Walsworth, M. Loncar, and A. Yacoby, A robust scanning diamond sensor for nanoscale imaging with single nitrogen-vacancy centres, *Nature nanotechnology* **7**, 320 (2012).
- [22] T. Van der Sar, F. Casola, R. Walsworth, and A. Yacoby, Nanometre-scale probing of spin waves using single electron spins, *Nature communications* **6**, 1 (2015).
- [23] C. Du, T. Van der Sar, T. X. Zhou, P. Upadhyaya, F. Casola, H. Zhang, M. C. Onbasli, C. A. Ross, R. L. Walsworth, Y. Tserkovnyak, *et al.*, Control and local measurement of the spin chemical potential in a magnetic insulator, *Science* **357**, 195 (2017).
- [24] H. Wang, S. Zhang, N. J. McLaughlin, B. Flebus, M. Huang, Y. Xiao, E. E. Fullerton, Y. Tserkovnyak, and C. R. Du, Quantum sensing of spin transport properties of an antiferromagnetic insulator (2020), arXiv:2011.03905 [cond-mat.mes-hall].
- [25] N. Bazazzadeh, M. Hamdi, F. Haddadi, A. Khavasi, A. Sadeghi, and S. Mohseni, Symmetry enhanced spin-nernst effect in honeycomb antiferromagnetic transition metal trichalcogenide monolayers, *Physical Review B* **103**, 014425 (2021).
- [26] K. Shen, Magnon spin relaxation and spin hall effect due to the dipolar interaction in antiferromagnetic insulators, *Physical Review Letters* **124**, 077201 (2020).
- [27] W. Xing, L. Qiu, X. Wang, Y. Yao, Y. Ma, R. Cai, S. Jia, X. Xie, and W. Han, Magnon transport in quasi-two-dimensional van der waals antiferromagnets, *Physical Review X* **9**, 011026 (2019).
- [28] M.-W. Lin, H. L. Zhuang, J. Yan, T. Z. Ward, A. A. Puretzky, C. M. Rouleau, Z. Gai, L. Liang, V. Meunier, B. G. Sumpter, *et al.*, Ultrathin nanosheets of crsite_3 : a semiconducting two-dimensional ferromagnetic material, *Journal of Materials Chemistry C* **4**, 315 (2016).